

***In Situ* Neutron Diffraction Study of the Electrochemical Intercalation of Potassium into Graphite in a Dimethyl Sulfoxide Solvent**

B. MARCUS AND PH. TOUZAIN

*Science des Surfaces et Matériaux Carbonés, Laboratoire Associé au CNRS
UA 413, ENS d'Electrochimie et d'Electrometallurgie, INPG, BP 75
Domaine Universitaire, 38402 Saint-martin d'Hères Cedex, France*

Received June 10, 1987; in revised form May 13, 1988

The stage transitions in ternary potassium-dimethyl sulfoxide-graphite intercalation compounds were observed by neutron diffraction measurements *in situ*, during the electrochemical intercalation of solvated potassium into graphite. The position and the profiles of the (00*l*) diffraction lines indicate first the formation of disordered stages for all compositions when the stage value is higher than that of stage 2, and second the coexistence of stage 2 and stage 1 during the last transition only. In the disordered (mixed) stages the ratio (n packages/ $n + 1$ packages) is found to vary continuously as the potassium concentration increases. These results have been compared to recent works on stage transitions in binary potassium-graphite intercalation compounds, as well as to the electrochemical intercalation of anions in graphite. © 1988 Academic Press, Inc.

I. Introduction

Staging is a remarkable feature revealed by the graphite intercalation compounds (GICs), in particular in the presence of heavy alkali metal atoms. The ordered sequence of one intercalate and n graphene layers ($n \geq 1$) has been observed for decades (1), but this ability to grow in sequential stages observed by diffraction measurements is not clear yet. In order to examine the different stage stabilities, several recent studies have focused their observation on stage transitions induced either by hydrostatic pressure applied to binary potassium GICs (2, 3) or by variation of the alkali metal concentrations in the graphite host lattice (4-6). The stage transitions related to the in-plane density of the intercalate

may be explained by the cation diffusion between the graphene layers as seen in the Daumas and Herold model (7). According to this domain wall theory, the transformations should occur via intermediate states corresponding to the overlapping of different stage-domains which should cause a c axis disorder. Such staging disorders—due to the stage $n \rightarrow$ stage $n - 1$ transition—are expected to be more easily observed when there is a diffuse scattering or (00*l*) diffraction line broadening. However, the different data from the above-mentioned works are quite confusing since some authors observed disordered (4) or fractional stages (2, 6) during the transition process while other teams reported only the coexistence of the two well-ordered pure stages throughout all the stage transitions (3, 5).

Moreover, these different results do not allow us to conclude whether elastic or electrostatic interactions are predominant for the staging occurrence in the GICs, as predicted by theoretical works (8–11). All these stage transformations were performed on binary potassium GICs. It was interesting to study the stage transitions in ternary potassium–solvent–GICs where the greater value of the intercalate size (d_0 parameter) is expected to enhance the elastic strains in graphene layers while the electrostatic interactions can be modified by the organic molecules.

In this paper, we report an observation of stage transitions in the ternary potassium–dimethyl sulfoxide–GICs obtained via cathodic reduction of a graphite electrode within a dimethyl sulfoxide (DMSO) solution of potassium salt.

The electrochemical synthesis of this ternary compound was first reported by Besenhard *et al.* (12, 13). They observed two steps in the potential/electrochemical charge curve corresponding to the successive formation of a second, then a first, stage which were characterized by their d_n parameters ($11.60 + n * 3.35 \text{ \AA}$) and their respective $\text{K}(\text{DMSO})_6\text{C}_{48}$ and $\text{K}(\text{DMSO})_6\text{C}_{24}$ stoichiometries. Moreover, they were able to observe via X-ray diffraction measurements four different stage compounds: $n = 1, 2, 3, 4$.

From gravimetric analysis, Okuyama *et al.* (14) attributed the two steps to the two $\text{K}(\text{DMSO})_3\text{C}_{48}$ (stage 4) and $\text{K}(\text{DMSO})_3\text{C}_{24}$ (stage 2) phases.

Fretigny *et al.* (15) have reported the formation of a golden compound, a color characteristic of the KC_8 binary phase.

Except for the last mentioned study, all these results show that the electrochemical method is convenient to observe stage transitions in ternary graphite compounds since the organic molecules solvating the ions are also inserted (16), resulting in a very large spacing between graphene layers. Depend-

ing on the solvent, d_0 varies from 5 to 10 \AA while the d_0 value in the binary potassium GIC is only 2.0 \AA .

The characterization of the different phases appearing during the electrochemical reduction of graphite was achieved by means of X-ray diffraction and chemical analysis. Then, in order to study the stage transitions in these ternary compounds and to compare them to the transitions reported for the binary compounds, we carried out the electrochemical synthesis of K – DMSO –graphite, and simultaneously recorded the structural changes of the graphitic electrode by “*in situ*” neutron diffractometry. This technique allowed us to analyze the whole sample owing to the weak absorption cross section of nuclei in the case of neutrons and to observe the integral changes during the intercalation reaction (17).

II. Experimental

The intercalation reaction was performed by cathodic reduction of a graphite electrode within an electrolytic solution of KClO_4 1 M in DMSO solvent.

Graphitic electrodes, constituted by samples of pressed powder or highly oriented pyrolytic graphite (HOPG) platelets, were attached to a platinum lead and were used as a working electrode. The counter electrode was a platinum wire while the reference one was a Ag/AgCl_2 electrode (18).

DMSO was stored over NaH powder before distillation. KClO_4 was dried for several hours at 120°C in vacuum before being solved in DMSO.

The experimental cell was achieved within dry argon. Reduction was carried out at room temperature under constant current conditions, with a “Tacussel PRT 20-2X” potentiostat. X-ray diffraction (XRD) spectra of the compounds were recorded with a Philips diffractometer using $\text{CuK}\alpha$ radiation.

For the neutron diffraction measurements, the advancement of the reaction was simultaneously studied via the potential/time curve and the diffraction spectra, recorded on the multidetector of the D₁B neutron diffractometer (ILL HFR Grenoble), at a wavelength of 2.517 Å. The HOPG sample (195 mg, size: 10 * 10 * 1 mm) was immersed in hexadeuterodimethyl sulfoxide in order to avoid neutron diffusion by hydrogen atoms. It was reduced under a 300 μA constant current. Meanwhile, the cell was normally rotated to the neutron incident beam direction and each diffraction peak recorded for 30 sec. The pressed powder sample ($\phi = 100 \mu\text{m}$ size: 12 mm diameter pellet of 720 mg) was reduced under 1 mA. The integral diffraction spectra were recorded every hour.

III. Results and Discussion

III.1. Sample Characterization

Figure 1 shows the electrochemical potential of a HOPG electrode recorded during constant reduction. The same variations in this curve were obtained with different graphite samples, Ceylan graphite powder or thin Madagascar graphite powder, and with different current values ranging from 2 to 10 μA/mg of graphite. The different fig-

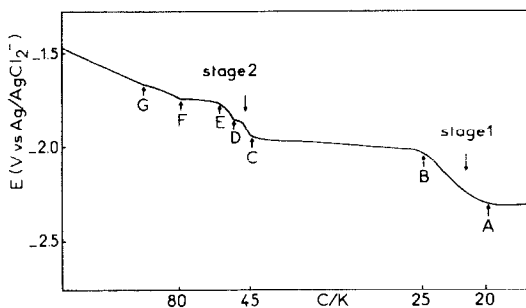


FIG. 1. Variation of the cell potential with the C/K molecular ratio during the reduction of graphite in 1 M potassium perchlorate-dimethyl sulfoxide solution.

TABLE I
EXPERIMENTAL VALUES OF d_n PARAMETERS (XRD) AND C/K RATIOS FROM CHRONOPOTENTIOMETRY AND CHEMICAL ANALYSIS

Points	d_n (Å) ^a	Stage <i>n</i>	C/K		
			<i>b</i>	<i>c</i>	<i>d</i>
G	25.00	4	110-120		
F	21.65	3	75-80	75 ± 2.5	90 ± 10
E	18.20	2	55-58		
D	18.20	2	51-54	46 ± 1.5	53 ± 5
C	18.20	2	45-47	40 ± 1.3	46 ± 4
B	14.95	1	25-26		
A	14.95	1	20-21	18 ± 0.6	20 ± 2

^a ± 0.05 Å.

^b From chronopotentiometry.

^c From flame spectroscopy analysis.

^d With a corrective term due to surface wetting by 2.5×10^5 mole K/cm² (corresponding to 10⁻⁵ liters of electrolyte).

ures reveal plateaus and step features characterized by several periods (G to A). The C/K ratios corresponding to these points have been calculated assuming a 100% current coulombic yield. They are listed in Table I with the related stage index and d_n parameters obtained from XRD spectra. All these results agree with the work as reported by Besenhard *et al.* (13). The C/K ratios were also determined by flame spectroscopy analysis after complete oxidation of the intercalated sample in perchloric acid. Table I confirms the good efficiency of the electrochemical intercalation since the results are quantitatively in agreement with the entire range of potassium concentration. The systematic difference may be explained by the wetting of the sample surfaces by the previously mentioned potassium electrolyte, which leads to higher values for the potassium contents, or by some binary golden-colored domains on the sample surface as reported by Fretigny *et al.* (15).

The d_n parameters were calculated for each phase from the (00*l*) Bragg reflection

TABLE II
XRD OF K(DMSO)_yC₂₀ FIRST STAGE COMPOUND

θ (°)	d (°)	001	I/I_0 exp (%)
13.95	7.36	002	11.0
20.87	4.936	003	34.5
28.00	3.710	004	100.0
35.10	2.966	005	12.5
42.40	2.473	006	11.0
49.86	2.121	007	4.0
57.60	1.856	008	5.0

positions (Table II). All stage present the same spacing between the two graphene layers adjacent to an intercalated layer: $d_0 = d_n - 3.35 n = 11.60 \pm 0.05 \text{ \AA}$, suggesting that the structure of the intercalated layer remains constant at every stage. The solvation number y of stage 1 has been determined by thermogravimetry. The loss of mass between 60 and 120°C, typical of the DMSO solvent evolution leads to $y = 6 \pm 0.25$. This solvation number has also been calculated for every stage assuming that the volume between two graphene layers was filled with liquid DMSO or with solid DMSO (19) (Table III). The results (close to $y = 6$) are in agreement with the previous work of Besenhard *et al.* (13), but it is surprising this number increases in relation with stage. This is inconsistent with the d_0 observed constant spacing for each phase and attributed to a similar structure of the intercalated layer. Two alternative explanations may be proposed:

(1) As found by Jegoudez *et al.* (20) on the graphite–potassium–furan system, the volume of the organic solvent increases as a function of the stage number, an increase probably due to the evolution of the electronic transfer between potassium and the furan molecule.

(2) The stage index, n , determined by XRD does not represent the integral sample structure, but only the ordered part of the

cathode which can diffract. As these stage-ordered domains decrease in number as potassium concentration goes down, the stage index value used for the y calculation must be corrected particularly in the case of higher stages.

On the other hand, the pseudo-plateau of the stage 2 region (D point) has also been observed during the overcharging of the second stage during the anodic oxidation of graphite by H₂SO₄ (21) and by AsF₆⁻ in nitromethane (22). It corresponds to the same XRD spectrum as for the C point ((001) lines of stage 2 only) when two diffraction peak sets were expected. Besenhard and Fritz (16) suggested that two different second stage phases with a close d_n parameter would coexist in this region.

In order to analyze the possible coexistence of two second stage phases and to study the stage transitions, we have carefully analyzed the profiles of the diffraction peaks recorded during the electrointercalation of solvated potassium ions.

III.2. Structural Study of the Compounds during the HOPG Platelet Reduction

Figures 2a and 2b respectively show the intensity variation of a (001) diffraction line for each stage appearing during the reaction and the simultaneous variation of the cell

TABLE III
IN-PLANE DENSITIES (ϵ) AND SOLVATION NUMBER (y)

Points	C/K	$\epsilon = \frac{K \cdot n}{C} (10^2)$	y^a	y^b
F	78	3.85	6.65	7.4
E	56	3.57	7.16	8.0
D	52	3.85	6.65	7.4
C	46	4.35	5.9	6.6
B	24	4.17	6.1	6.8
A	21	4.76	5.35	6.0

^a Calculated with the liquid density of DMSO.

^b Calculated with the solid density of DMSO.

potential. The Bragg reflections related to the stage sequence were fitted to Gaussian functions, and the intensity was calculated as an integral function. The successive recorded spectra confirm that the plateaus correspond to two sets of (00 l) diffraction lines, while the steps are only due to one crystallographic phase. Under our experimental conditions, the (002) graphite Bragg peak has fully disappeared before reaching G point on the curve; so, before stage 4 formation, the integral volume of the cathode is already transformed allowing the estimation of "sliding" rate close to 2×10^{-5} cm/sec for the solvated potassium ions. Thus, this high rate will not be a intercalation-process limitant factor.

Stage $n \rightarrow$ stage $n - 1$ transition study ($n > 2$). A careful examination of the peak

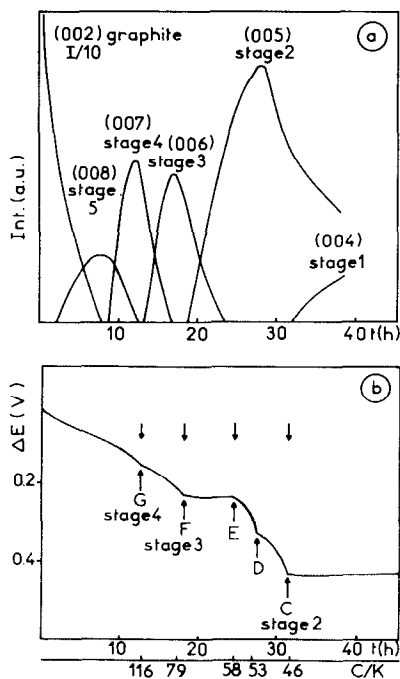


FIG. 2. Intensity variation of a (00 l) diffraction line for each stage appearing during the reduction of a HOPG platelet in 1 M potassium perchlorate-dimethyl sulfoxide (a) and simultaneous variations of the cell potential (b).

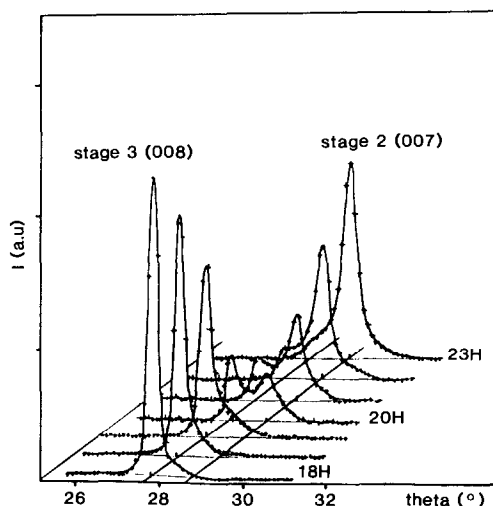


FIG. 3. Evolution of one part of the diffraction spectra during the stage 3 \rightarrow stage 2 transition in a HOPG.

shapes reveals that the diffraction lines do not always appear as a Gaussian or a Lorentzian function, particularly in the two-phase areas. Figure 3 gives an example of the diagram evolution between $\theta = 26^\circ$ and 32° , recorded during the stage 3 \rightarrow stage 2 transition in the F-E domain of the electrochemical curve. Under our experimental conditions, this transformation was completed after some 7 hr. This part of the diffraction spectra shows the decrease of the (008) stage 3 line and the growth of the (007) stage 2 one, depending on the potassium concentration varying between the $\text{K}(\text{DMSO})_6 \text{C}_{79}$ and $\text{K}(\text{DMSO})_6 \text{C}_{57}$ compositions.

Nevertheless, if the spectra seem to originate from the presence of two distinct phases, we failed in fitting the observed overlapping profiles to two Gaussian or Lorentzian functions, centered on the known positions for the (008) stage 3 and (007) stage 2 reflections, as would be expected if these two pure phases coexisted (Fig. 4a). However, the combined profiles were in good agreement with the superposition of three independent Gaussian

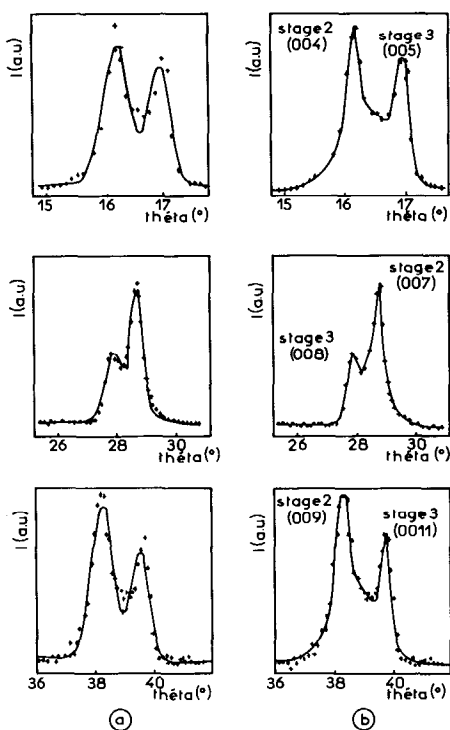


FIG. 4. Observed profiles (+++) fitted via two Gaussian functions (a) and via three Gaussian functions (b) during the stage 3 \rightarrow stage 2 transition in a HOPG platelet.

lineshapes resulting from the following adjustments:

—Two sharp diffraction peaks (at fixed θ) corresponding to the two expected values of the diffusion vectors for the (008) stage 3 and (007) stage 2 Bragg reflections.

—A wider line with a position depending on the potassium concentration and shifting from the (008) stage 3 position to the (007) stage 2 one.

The same spectrum evolution has been observed for other (00 l) diffraction peaks when the two diffusion vectors of the two successive stages are close to each other (Fig. 4b). Metz and Hohlwein (23) observed such a crystallographic behavior for FeCl₃ GICs. According to the experimental con-

ditions, they obtained microscopic mixtures (or solid solutions) of stages characterized by a noninteger ratio of graphene and intercalated layers. For these noninteger stage compounds, the diffraction diagrams reveal Bragg reflections whose q vector values have shifted away from the q vector values of pure stages, as modeled by Hendricks and Teller (24).

These results can then be described by the coexistence of three distinct crystallographic domains: separated domains for pure stage 3 and for pure stage 2, and another one for statistical mixtures of these two phases. The continuous shift of the q vectors indicates that (in these domains of microscopic mixtures of the two stages), the amount of stage 3 packets is continuously decreasing from 100 to 0%, while the stage 2 packets become more and more numerous while the potassium concentration is increasing.

Figure 5a represents, as a function of time, the relative amount of the two pure phases and of the mixed phase, based on the (00 l) integrated intensities; as for Fig. 5b, it shows the simultaneous change of the full width at half height (FWHM) of each peak throughout the stage transformation. It can be seen that the number of pure stage crystallographic domains are continuously evolving, while the c axis parameter deduced from the peak positions remains constant. It is also noteworthy that the pure stage peaks do not broaden as their intensities vary. These data indicate that the pure stages keep the same organization, perpendicular to the layers, and are not disordered by the potassium concentration change during the stage transition. Only the respective amount of the two phases varies, as also observed during the stage transitions in binary K-GICs (3, 5).

Contrarily, the diffraction lines of the nonpure stages present an important widening characteristic of a disorder enhancement of these mixed domains.

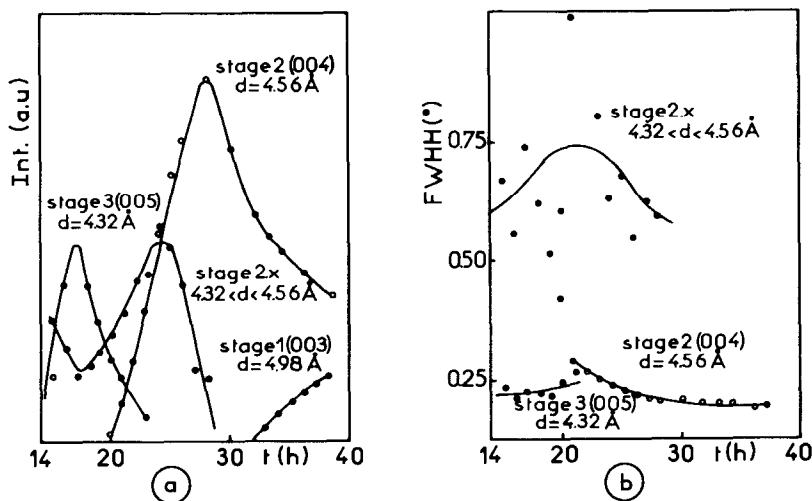


FIG. 5. Intensity (a) and FWHM (b) variation of (005) stage 3, (004) stage 2, and (001) mixed stage diffraction peaks during the stage 3 \rightarrow stage 2 transition in a HOPG platelet.

These observations agree with a domain growth according to the Daumas–Herold model (7). Figure 6 represents such a mechanism for the stage 3 \rightarrow stage 2 transition. The broad solid solution peaks can be seen as a set of numerous reflections due to intermediary nonpure stages.

The same phenomenon was observed throughout the stage 4 \rightarrow stage 3 transition (Fig. 7), corresponding to the $K(DMSO)_6 C_{120}$ – $K(DMSO)_6 C_{80}$ composition range. Nevertheless, if the different (00 l) overlap

profiles fit very well to three Gaussian functions, the mixed phase/pure phase intensity ratios are here more important than during the stage 3 \rightarrow stage 2 transition, indicating

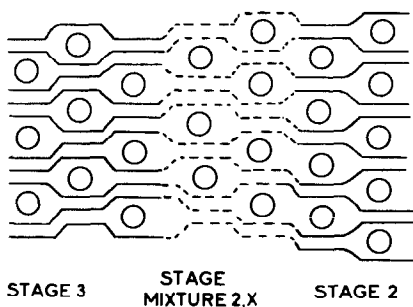


FIG. 6. Schematic representation (from the Daumas and Herold (7) model), of the stage 3 \rightarrow stage 2 transition.

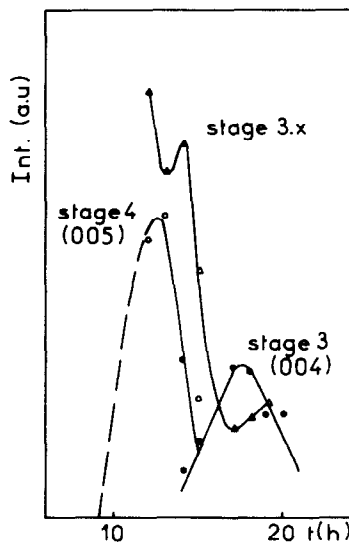


FIG. 7. Intensity variation of (005) stage 4, (004) stage 3, and (001) mixed stage diffraction peak during the stage 4 \rightarrow stage 3 transition in a HOPG platelet.

large domains of nonpure stage in the low potassium concentration range. Misenheimer and Zabel (4) reported the same behavior during the intercalation of potassium vapor into graphite.

Stage 2 evolution study. A careful examination of the (00 l) diffraction lines, recorded during the step corresponding to the stage 2 stoichiometries (E–C part of the curve), has never shown a shift of these (00 l) reflections. During the pseudo-plateau observed in this step (around D point), no transition was noticed between the two phases of stage 2 with different d_2 parameters, whereas the vanishing of the mixed phase domains was observed (Fig. 5a). The first part of the step (E–D) corresponds to the coexistence of solid solution and pure stage 2 domains, while during the second part (D–C), pure stage 2 only exists. At C point, the (00 l) stage-1-phase Bragg reflections begin to grow.

Stage 2 \rightarrow stage 1 transition study. At this time, the diffraction spectra are represented by only two sets of Gaussian lineshapes corresponding to the diffraction lines of pure stage 2 and stage 1. The stage 2 (00 l) Bragg reflections decrease as the first stage ones increase, but no broadening was observed; the width of the first stage reflections is limited to the instrumental resolution. The long-range order along the c axis of the two coexisting phases is not disturbed by this transformation, as reported

for the stage transitions in the binary potassium–GICs (3, 5). The integral transformation observed during the reduction is fully comparable to the recent data reported by Misenheimer and Zabel (4) for the binary compounds: phase transitions were found to occur via disordered stages for $n + 1$ stage to n stage shift (with $n > 2$), while during the stage 2 to stage 1 last transition we only observed the coexistence of the two pure stages.

Domain size study. The domain sizes are calculated from the width of the different (00 l) diffraction lines with Scherrer's equation:

$$D_n = \lambda/\beta \cos \theta,$$

where β represents the (00 l) diffraction line widths compared to the instrumental resolution at the same θ value (Table IV).

The c axis order increases with the potassium concentration both for the pure stages and for the mixed ones; however, this order is greater in pure phases than in mixed ones.

III.3. Structural Study of the Compounds during the Graphite Powder Reduction

(00 l) Diffraction line study. The powder diffraction spectra are quite different from those recorded in the case of the HOPG platelet until the $K(\text{DMSO})_6\text{C}_{45-47}$ stage 2 composition appears: we observed a set of large (00 l) Bragg reflections with a variable 2θ position. The variation of the d_n parameter, calculated from the variation of the (00 l) position as a function of the potassium concentration, is plotted in Fig. 8. The so-determined cell parameter is in good agreement with the calculated d_n parameter in the HOPG solid solution domains for the same potassium concentrations, and is found to vary continuously as predicted by Kirczenow (11).

Inversely, on the C–B plateau corresponding to stoichiometries ranging from stage 2 to stage 1, we have recorded the two

TABLE IV
SIZE DOMAINS ALONG THE c AXIS

Stage n	d_n (Å)	d_{n-n+1} (Å)
4–5		300
4	1400	
3–4		500
3	1700	
2–3		1000
2	2000	
1	>2000	

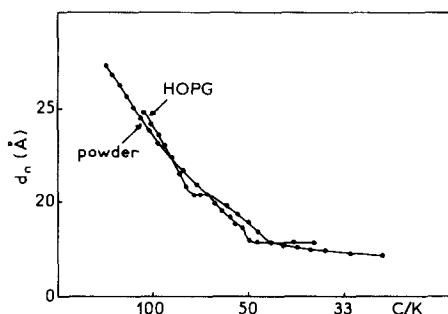


FIG. 8. Variation of the d_n parameter calculated from the (001) diffraction line position in the powder sample compared with the calculated d_n parameter in the solid solution domains of the HOPG platelet.

sets of (00 l) diffraction lines for the two pure phases, as during the HOPG reduction. The reduction reaction in small crystallites is fully comparable to the reduction reaction in the HOPG sample: regardless of the sample size and geometry, stage-mixture domains are observed during higher stages to stage 2 transitions, but are never recorded during the last one (stage 2 \rightarrow stage 1).

(100) Diffraction line study. Figure 9 presents the (100) Bragg reflection position and its FWHH as a function of the potassium content. The d_{c-c} distances in the graphene layers, deduced from the (100) reflection positions, are also indicated on this figure. It can be seen that the (100) peak position remains nearly unchanged from graphite phase to stage 3, and begins to shift toward a higher reticular distance when stage 2 is growing. Meanwhile, the (100) FWHH increases until stage 3 appears. The final width at stage 2 is comparable to the initial graphite FWHH and may be explained by only one C–C distance, the same in all planes, while the linewidth observed before stage 2 would result from different in-plane C–C distances, some in the graphene layers adjacent to the intercalated planes and some in the more distant and less disturbed graphene layers. However, it

is not explained why the d_{c-c} value is not changed from graphite to stage 3, although—even in the highest stages—some of the graphene layers are adjacent to intercalated planes.

IV. Conclusions

The electrochemical synthesis of the ternary potassium–dimethyl sulfoxide–GICs has been performed by means of the graphite cathodic reduction method.

The variation of the cell potential with the potassium content shows successive steps attributed to one stage domains and plateaus recorded between two steps related to transition regions as always observed in graphite electrochemical reduction or oxidation.

Stage compositions have been found to vary around the $K(DMSO)_6C_{24n}$ value as reported by Besenhard *et al.* (12, 13), with d_n parameter equal to $(11.55 + 3.35n)$ Å, where n is the stage index. However, all observed stages present a range of stoichiometry around the ideal in-plane density $\varepsilon = 1/24$; for example, the stage 1 composition varies from $K(DMSO)_6C_{20-21}$ to $K(DMSO)_6C_{24-25}$.

The pseudo-plateau observed in the stage 2 region of the electrochemical curve, also recorded during the electrochemical inter-

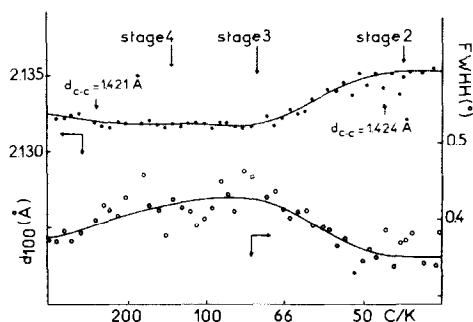


FIG. 9. Variation of the (100) reticular distance and of the (100) FWHH, during the reduction of the powder sample.

calation of anions (21, 22), coincides in our experiment with the vanishing of the (00 l) diffraction lines of the disordered domains.

The stage transformations, leading to the first stage, have been studied via *in situ* neutron scattering. For the n stage- $n - 1$ stage transitions ($n > 2$) we have simultaneously observed disordered domains of microscopic mixtures for both stages, as well as two well-ordered stage domains, while during the stage 2 \rightarrow stage 1 transition, the coexistence of the two pure stages only was observed. The (00 l) peak positions of the solid solution domains are found to vary continuously when the potassium content is increasing. Similar (00 l) diffraction spectra were observed for the HOPG and the powder sample with the same potassium concentrations. As the intercalation rate is not here a limitant factor, the stage mixture or pure stage formation is not due to the "sliding" effect related to the intercalation process, but only depends on the intercalate concentration. Misenheimer and Zabel (4) reported a fully comparable behavior of the stage transition process in binary potassium-GICs. However, the effect of the intercalate size on the domain walls may explain why the K/DMSO ternaries seem to be more disordered than the alkali binaries: the interlayer spacing is considerably larger, hence the Daumas and Herold boundaries will represent a more serious perturbation. This intercalate size may also explain the formation of a fractional stage $n = 4/3$ in a similar experiment where the synthesis of ternary potassium-tetrahydrofuran-graphite compounds was carried out (6). In this system, the intercalate thickness ($d_0 = 5.55 \text{ \AA}$) induces less perturbations in the domain walls than the large thickness ($d_0 = 11.6 \text{ \AA}$) observed in the case of DMSO intercalates. These changes in the elastic strains may involve different domain sizes, then different mechanism of transitions. This was theoretically predicted to occur by Kirczenow (25) with

a model based on a semiquantitative treatment which takes into account the domain sizes related to the "healing length" of the deformation induced by the intercalate.

Acknowledgments

We thank Dr. A. W. Moore (Union Carbide Co.) for providing the HOPG material, the Laue Langevin Institute (ILL Grenoble) for the experimental and technical support of the neutron diffraction measurements, and particularly Dr. J. J. Pannetier and J. L. Soubeyrou, and also J. Simonet for his valuable assistance.

References

1. V. HOFFMANN AND A. FRENZEL, *Z. Elektrochem.* **37**, 613 (1931).
2. C. D. FUERST, J. E. FISHER, J. D. AXE, J. B. HASTINGS, AND D. B. MCWHAN, *Phys. Rev. Lett.* **50**, 357 (1983).
3. R. CLARKE, N. WADA, AND S. A. SOLIN, *Phys. Rev. Lett.* **44**, 1616 (1980).
4. M. E. MISENHEIMER AND H. ZABEL, *Phys. Rev. Lett.* **54**, 2521 (1985).
5. R. NISHITANI, Y. UNO, AND H. SUEMASTU, *Phys. Rev. B* **27**, 6572 (1983).
6. B. MARCUS, PH. TOUZAIN, AND J. L. SOUBEYROUX, *Synth. Met.* **26**, 13 (1988).
7. N. DAUMAS AND A. HEROLD, *C.R. Acad. Sci.* **268**, 373 (1969).
8. S. A. SAFRAN, *Phys. Rev. Lett.* **44**, 937 (1980).
9. S. A. SAFRAN AND D. R. HAMANN, *Phys. Rev. Lett.* **42**, 1410 (1979); *Phys. Rev. B* **22**, 606 (1980); *Phys. B* **99**, 469 (1980); *Phys. Rev. B* **23**, 565 (1981).
10. S. E. MILLMAN AND G. KIRCZENOW, *Phys. Rev. B* **28**, 3482 (1983).
11. G. KIRCZENOW, *Phys. Rev. Lett.* **52**, 437 (1984); *Phys. Rev. B* **31**, 5376 (1985).
12. J. O. BESENHARD, *Carbon* **14**, 111 (1976).
13. J. O. BESENHARD, H. MOHWALD, AND J. J. NICKL, *Carbon* **18**, 399 (1980).
14. N. OKUYAMA, T. TAKAHASHI, S. KANAYAMA, AND H. YASUNAGA, *Phys. B* **105**, 298 (1981).
15. C. FRETIGNY, D. MARCHAND, AND M. LAGUES, *Proc. Int. Conf. Carbon, Baden-Baden*, 204 (1986).
16. J. O. BESENHARD AND H. P. FRITZ, *Angew. Chem. Int. Ed. Engl.* **22**, 950 (1983).
17. C. RIEKEL, *Prog. Solid State Chem.* **13**, 89 (1980).
18. J. COURTOT-COUCPEZ AND M. LE DEMEZEZ, *C.R. Acad. Sci. Paris* **65**, 2636 (1966).
19. R. THOMAS, C. B. SHOEMAKER, AND K. ERIKS, *Acta Crystallogr.* **21**, 12 (1966).

20. J. JEGOUDEZ, CH. MAZIERES, AND R. SETTON, *Carbon* **24**, 747 (1986).
21. A. METROT AND M. TIHLI, *Synth. Met.* **23**, 19 (1988).
22. D. BILLAUD, A. CHENITE, AND A. METROT, *Carbon* **20**, 493 (1982).
23. W. METZ AND D. HOHLWEIN, *Carbon* **13**, 87 (1975).
24. S. HENDRICKS AND E. TELLER, *J. Chem. Phys.* **10**, 147 (1942).
25. G. KIRCZENOW, *Synth. Met.* **12**, 143 (1985); *Phys. Rev. Lett.* **55**, 2810 (1985).